Chinese Chemical Letters 36 (2025) 109958

Contents lists available at ScienceDirect

Chinese Chemical Letters

journal homepage: www.elsevier.com/locate/cclet

Interfacial interactions of Cu/MnOOH enhance ammonia synthesis from electrochemical nitrate reduction

Hong-Rui Li, Xia Kang, Rui Gao, Miao-Miao Shi*, Bo Bi, Ze-Yu Chen, Jun-Min Yan*

Key Laboratory of Automobile Materials, Ministry of Education, School of Materials Science and Engineering, Jilin University, Changchun 130022, China

ARTICLE INFO

Article history:
Received 27 November 2023
Revised 5 April 2024
Accepted 30 April 2024
Available online 1 May 2024

Keywords:
Ammonia
Nitrate reduction reaction
Adsorption
Electrocatalysis
Interfacial interactions

ABSTRACT

In this work, an effective catalyst of Cu/MnOOH has been successfully constructed for electrochemical nitrate reduction reaction (eNO_3RR) for synthesis of ammonia (NH_3) under ambient conditions. The substrate of MnOOH plays an important role on the size and electronic structure of Cu nanoparticles, where Cu has the ultrafine size of 2.2 nm and positive shift of its valence states, which in turn causes the increased number of Cu active sites and enhanced intrinsic activity of every active site. As a result, this catalyst realizes an excellent catalytic performance on eNO_3RR with the maximal NH_3 Faraday efficiency (FE) (96.8%) and the highest yield rate (55.51 mg h^{-1} cm^{-2}) at a large NH_3 partial current density of 700 mA/cm^2, which could help to promote the industrialization of NH_3 production under ambient conditions.

Ammonia (NH_3), serving as industrial chemicals and energy carrier, exhibits great potential in agriculture and industry [1,2]. Nowadays, the production of NH_3 is heavily dependent on the energy-intensive Haber-Bosch approach, which is conducted at high temperature and pressure along with massive carbon dioxide (CO_2) emission [3,4]. As an alternative, the electrochemical pathway for NH_3 synthesis which is derived from nitrogen (N_2) and water (H_2O) under ambient conditions attracts much interest [5-9]. But the low NH_3 yield rate (<0.3 mg h^{-1} $mg_{cat.}^{-1}$) and poor Faraday efficiency (FE) (<71%) critically restrict its widespread application [10-12].

Compared with the inert N≡N bond, the N=O bond possessing relatively low dissociation energy displays much better reaction kinetics for electrochemical NH_3 production [13-16]. Therefore, nitrate (NO_3^-) can serve as an appropriate species for NH_3 synthesis. Besides, NO_3^- is the majority source of N-containing pollutants in industrial wastewater with high solubility [17,18]. Hence, the electrochemical NO_3^- reduction reaction (eNO_3RR) not only realizes renewable NH_3 synthesis but also accelerates the transformation of the nitrogen cycle.

The application of Cu, Ni, and Ru based catalysts in eNO_3RR has been reported; however, most of these catalysts display the limited current density and NH_3 yield rate [19-23]. Meanwhile, eNO_3RR is a reaction which involves multiple electrons and intermediates, and the hydrogen evolution reaction (HER) is a competition reaction during eNO_3RR, and thus the NH_3 FE faces significant challenges [19,24-26]. Previous studies have proposed various strategies to improve the performance of eNO_3RR [27,28]. Thereinto, surfaces with positive charge can accumulate anions due to the electrostatic attraction effect [29-32]. Therefore, atoms with positive charge might realize enhanced NO_3^- adsorption ability. It is worth noting that the introduction of substrate is one of the most effective strategies to tailor the electronic structure of catalysts, and then modulate the adsorption energy of the reactants and intermediates [33,34]. In addition, the anchoring and dispersing effects of the substrate can create more active sites towards NH_3 synthesis. Therefore, finding a suitable substrate to modulate the active center, such as Cu, may improve its catalytic performance for eNO_3RR.

Herein, we develop an effective eNO_3RR catalyst by anchoring Cu nanoparticles (NPs) on hydroxymanganese oxide (Cu/MnOOH) *via* a convenient reduction method. Due to the dispersion effect of MnOOH substrate, Cu NPs have a small average size of 2.2 nm, which leads to abundant active sites. In addition, the presence of MnOOH enables the charge of Cu a little positive shift, and the adsorption experiment shows that Cu/MnOOH exhibits much better adsorption capacity for NO_3^- as expected. Benefiting from the numerous active sites and enhanced adsorption capacity, Cu/MnOOH displays a high catalytic activity, which can achieve a maximal FE of 96.8%, and yield rate of 55.51 mg h^{-1} cm^{-2} at a large NH_3 partial current density of 700 mA/cm^2 for NH_3 synthesis. At the same time, during the 20 h of long-term electrolysis, the eNO_3RR performance does not decline over Cu/MnOOH catalyst.

* Corresponding authors.
E-mail addresses: miaomiaoshi@jlu.edu.cn (M.-M. Shi), junminyan@jlu.edu.cn (J.-M. Yan).

https://doi.org/10.1016/j.cclet.2024.109958
1001-8417/

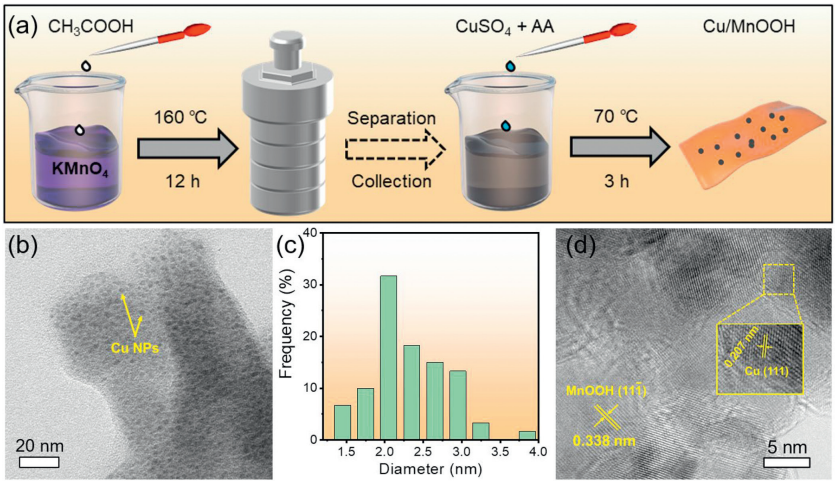

Fig. 1. (a) Schematic diagram of synthesizing Cu/MnOOH catalyst. (b) TEM image of Cu/MnOOH, and the corresponding (c) size distribution of Cu NPs and (d) HRTEM image of Cu/MnOOH.

Cu/MnOOH is synthesized *via* a two-step reaction involving hydrothermal treatment and reduction procedure (Fig. 1a). The loading mass of Cu on Cu/MnOOH is ~13.66 wt%, which is determined by inductively coupled plasma optical emission spectrometry (ICP-OES). The scanning electron microscopy (SEM) image reveals that the Cu/MnOOH and pure MnOOH exhibit a similar lamellar structure (Fig. S1 in Supporting information). However, some NPs can be observed through the transmission electron microscope (TEM) image in comparison with pure MnOOH (Fig. 1b and Fig. S2 in Supporting information), demonstrating the formation of Cu NPs on MnOOH. The average Cu particle size is 2.2 nm (Fig. 1c). In contrast, XC-72 carbon is also used as the substrate to disperse Cu NPs (Cu/C) through the same method (Fig. S3 in Supporting information), where the average particle size of Cu is 2.3 nm (Fig. S4 in Supporting information), which is similar to that of Cu/MnOOH. Fig. 1d shows the high-resolution TEM (HRTEM) image of Cu/MnOOH and the Cu (111) plane with a lattice spacing of 0.207 nm and MnOOH (11$\bar{1}$) plane with a lattice spacing of 0.338 nm can be observed. The lattice spacing of MnOOH (11$\bar{1}$) plane for Cu/MnOOH is consistent with that of pure MnOOH (Fig. S5 in Supporting information), suggesting the loading of Cu does not affect the crystal structure of the substrate.

As can be seen from the X-ray powder diffraction (XRD) pattern of Cu/MnOOH (Fig. 2a), there are obvious diffraction peaks located at 43.4°, 50.5°, and 74.2°, corresponding to (111), (200), and (220) crystal planes of metallic Cu (JCPDS No. 04-0836), respectively [35]. And the other peaks can be attributed to the crystallized MnOOH (JCPDS No. 41-1379) [36]. The Raman spectrum of Cu/MnOOH (Fig. 2b) exhibits bands in the range of 200–800 cm^{-1} that are consistent with MnOOH [37,38].

In general, the electronic state of the loading metal could be modified by the support, especially the particles in small size [39,40]. Therefore, X-ray photoelectron spectroscopy (XPS) characterizations are carried out to analyse the valence states and chemical compositions of Cu/MnOOH, pure MnOOH, and Cu/C catalysts. As shown in Fig. 2c, for Cu/C, the two prominent binding energies of Cu 2p are centered at 932.60 (Cu $2p_{3/2}$) and 952.41 eV (Cu $2p_{1/2}$), and Auger electron spectroscopy (AES) spectra of Cu LMM for Cu/C is located at 569.88 eV (Fig. S6 in Supporting information), confirming the presence of Cu^0 [35,41]. However, the binding energies of Cu 2p for Cu/MnOOH exhibit a positive shift compared to those for Cu/C, which are located at 932.74 and 952.55 eV, and Cu LMM AES spectra for Cu/MnOOH also have positive shift compared to Cu/C (570.01 eV, Fig. S6). Namely, MnOOH can modulate the electronic structure and valence states of metals (or

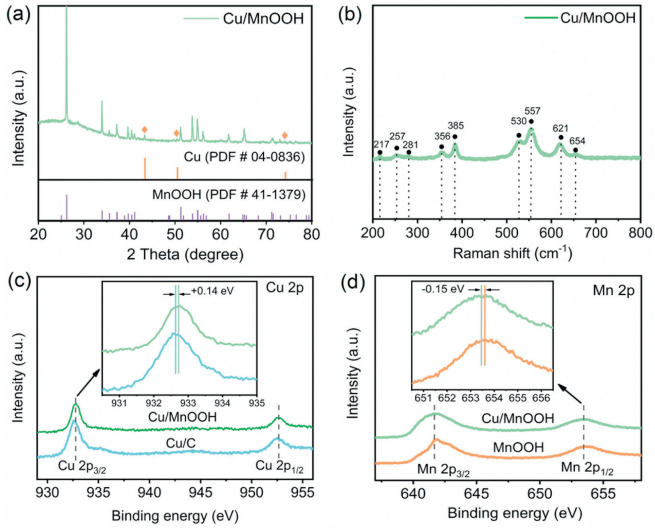

Fig. 2. (a) XRD pattern of Cu/MnOOH catalyst. (b) Raman spectra of Cu/MnOOH catalyst, and XPS spectra of (c) Cu 2p and (d) Mn 2p for Cu/MnOOH, Cu/C, and pure MnOOH.

metal oxides) through interfacial interactions as expected. This interaction between Cu and MnOOH positively regulates the valence shift of Cu NPs [42-44]. The Mn 2p spectra of pure MnOOH and Cu/MnOOH are shown in Fig. 2d. For pure MnOOH, the binding energies are centered at 641.95 (Mn $2p_{3/2}$) and 653.60 eV (Mn $2p_{1/2}$) [45]. The spin-orbit splitting value of Mn 2p binding energies (ΔE) is 11.65 eV, illustrating the possible existence of Mn^{3+} [46-48]. Owing to the formation of Mn^{3+}, considerable empty orbits might induce the electronic interactions between the Cu NPs and MnOOH substrate, leading to the positive shift of Cu binding energies [49]. On the other hand, the Mn 2p binding energies of Cu/MnOOH exhibit a negative shift relative to the pure MnOOH, with peaks observed at 641.80 and 653.45 eV. Both considering the binding-energy shift between Cu and Mn, the electron transfer does occur from Cu to Mn, which leads to the surface of Cu with a positive charge. And this positive charge may help to enhance its NO_3^- adsorption ability and thus increase the catalytic activity for eNO_3RR (*vide infra*).

To investigate the effect between Cu and MnOOH, pure MnOOH and Cu/C are also tested as control samples. The catalysts are all evaluated under identical conditions, employing carbon cloth

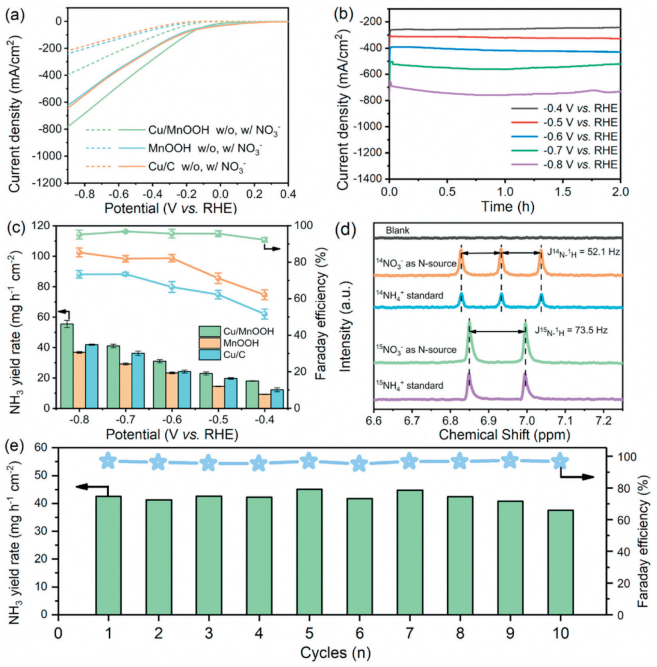

Fig. 3. (a) LSV curves of Cu/MnOOH, Cu/C, and pure MnOOH catalysts. (b) Chronoamperometry curves for Cu/MnOOH catalyst at different potentials with 0.5 mol/L NO_3^- and 1.0 mol/L KOH. (c) NH_3 yield rates and FEs of Cu/MnOOH, Cu/C, and pure MnOOH catalysts. (d) ^1H NMR spectra of NH_4^+ standard solution and electrolyte after eNO_3RR with Cu/MnOOH catalyst at −0.8 V, and (e) recycle stability of Cu/MnOOH for 10 runs at −0.7 V.

as the current collector. Initially, linear sweep voltammetry (LSV) measurements are performed in (KOH, 1.0 mol/L) electrolyte solution with or without the presence of NO_3^- (0.5 mol/L). The presence of NO_3^- leads to an enhanced current density for all samples, while Cu/MnOOH exhibits the highest current density at the same potential, indicating its superior catalytic performance towards eNO_3RR (Fig. 3a). Chronoamperometry (CA) tests at various potentials are conducted to evaluate the NH_3 yield rates and FEs, and the produced NH_3 is quantified by the indophenol blue method (Fig. S7 in Supporting information) [19]. Fig. 3b presents the current density of Cu/MnOOH at different potentials in KOH (1.0 mol/L) and NO_3^- (0.5 mol/L). The current density exhibits an increase with the negative shift of potentials within the potential range of −0.4 V to −0.8 V, and the NH_3 partial current density can reach a maximum value of 700 mA/cm^2 at −0.8 V. After electrolysis for 2 h, the NH_3 production is tested by ultraviolet-visible (UV–vis) spectrophotometry (Fig. S8 in Supporting information). The results demonstrate that all FEs achieved with the catalyst of Cu/MnOOH at the given potentials exceed 90%, with the highest value reaching an impressive 96.8% at −0.7 V (Fig. 3c). Additionally, the NH_3 yield rate reaches a remarkable value of 55.51 mg h^{-1} cm^{-2} at −0.8 V, outperforming the majority of the reported ones, and the energy consumption is comparable to other reported ones (Table S1 in Supporting information). In contrast, at −0.8 V, pure MnOOH exhibits its optimum NH_3 yield rate (36.85 mg h^{-1} cm^{-2}) and FE (85.3%), which are comparatively inferior to those of Cu/MnOOH, and the beneficial influence of Cu NPs is thus emphasized. In addition, Cu/C exhibits the lower eNO_3RR performance with the optimum NH_3 yield rate of 41.93 mg h^{-1} cm^{-2} and FE of 73.4% at −0.8 V, demonstrating that MnOOH substrate could efficiently promote the activity and selectivity for NH_3 synthesis from eNO_3RR. It should be noted that the possible gaseous NH_3 is also collected by acid absorbent (0.1 mol/L HCl), and the results demonstrated that the leakage of the gaseous NH_3 is proved to be negligible (Table S2 in Supporting information). Therefore, all eNO_3RR processes are conducted in a sealed cathode chamber.

Besides NH_3, the possible by-product of NO_2^- is also detected which is derived from the desorption of adsorbed nitrite (NO_2^*) intermediate. And the determination of produced NO_2^- is used the *N*-(1-naphthyl)ethylenediamine dihydrochloride coloration method (Fig. S9 in Supporting information). Notably, the FEs of eNO_3RR to the products of NH_3 and NO_2^- are nearly 100% in the potential range of −0.4 ∼ −0.8 V, suggesting that eNO_3RR can surpass the competing HER (Fig. S10 in Supporting information), further demonstrating the enhanced selectivity of Cu/MnOOH towards NO_3^-. To prevent the impact of pollutants on results, the electrolyte with NO_3^- before electrolysis and the electrolyte without NO_3^- after electrolysis is also tested. Fig. S11 (Supporting information) displays that only the electrolyte with NO_3^- after electrolysis can detect NH_3 product, suggesting the produced NH_3 is derived from NO_3^-.

To confirm the accuracy of the generated NH_3, the NH_3 yield is also detected by ^1H-nuclear magnetic resonance (NMR). As shown in Fig. 3d, three peaks with the coupling constant of $J_{^{14}N-^1H}$ = 52.1 Hz (*J* is determined by the product of the difference between the chemical shifts of two neighbouring peaks and the strength of the instrumental magnetic field) corresponding to $^{14}NH_4^+$ are observed obviously with NO_3^- (0.5 mol/L) after 2 h electrolysis at −0.8 V, which is consistent with the standard $^{14}NH_4^+$ solution [50,51]. According to the calibration curves of ^1H NMR in Fig. S12 (Supporting information), the NH_3 yield rate is 56.06 mg h^{-1} cm^{-2} (Fig. S13 in Supporting information). Remarkably, this result agrees well with that obtained through UV–vis spectroscopy. Additionally, the isotopic labeled $^{15}NO_3^-$ is further used for eNO_3RR [52], and two peaks with the coupling constant of $J_{^{15}N-^1H}$ = 73.5 Hz corresponded to $^{15}NH_4^+$ are also observed (Fig. 3d) [50], confirming that the generated ammonia is originated from the added NO_3^- but not from air or other sources of N.

Durability is an important property of a catalyst, and thus a long-term experiment is conducted to demonstrate the excellent stability of Cu/MnOOH at −0.7 V. Considering that the NO_3^- would be consumed gradually during the eNO_3RR process, fresh electrolyte (0.5 mol/L NO_3^- and 1.0 mol/L KOH solution) is replaced every two hours. As a result, the NH_3 yield rates and FEs could maintain stable for 10 cycles (20 h) (Fig. 3e), and further characterizations demonstrate that Cu/MnOOH possess good structural stability (Fig. S14 in Supporting information). This might be due to the anchoring effect of MnOOH which prevents the growth and agglomeration of Cu NPs. Additionally, it should be noted that the pH of the electrolyte can maintain stable before (13.84) and after (13.92) reaction (Table S3 in Supporting information), which is beneficial to the stability of the catalyst.

To further investigate the good performance of Cu/MnOOH, a series of experiments are carried out. Through the results of electrochemical impedance spectroscopy (EIS) (Fig. 4a), Cu/MnOOH shows a much lower charge transfer resistance than those of pure MnOOH and Cu/C, and this means that Cu/MnOOH has a good electron-transfer capability during eNO_3RR, leading to the higher activity of Cu/MnOOH for NH_3 synthesis. The eNO_3RR process involves multiple steps, including adsorption of NO_3^-, hydrogenation, electron transfer. The adsorption ability of Cu/MnOOH, pure MnOOH, and Cu/C to NO_3^- are determined by comparing the concentration difference of NO_3^- in the solution before and after soaking treatment, and the experimental details are provided in Supporting information [53]. The concentration of NO_3^- is tested by UV–vis spectrophotometer (Fig. S15 in Supporting information). The adsorption results (Fig. 4b) demonstrate that Cu/MnOOH has the highest adsorption capacity towards NO_3^-, and the quantity of adsorbed NO_3^- (q_e) in NO_3^- solution (0.5 mol/L, 25 mL) for 2 h can

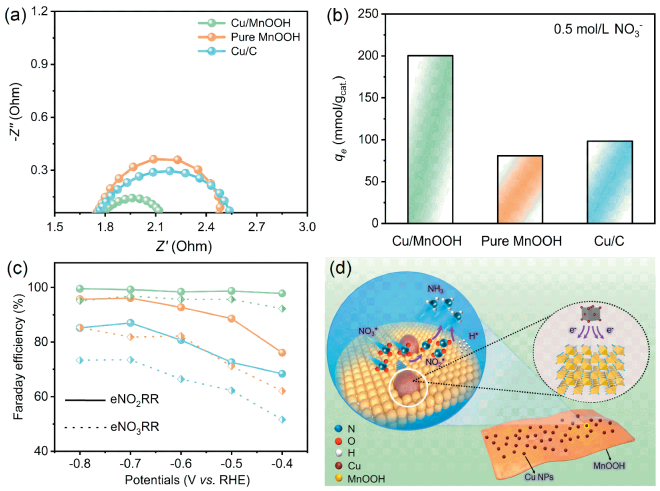

Fig. 4. (a) EIS measurements of Cu/MnOOH, pure MnOOH and Cu/C under the same condition. (b) Adsorption capacities of Cu/MnOOH, pure MnOOH and Cu/C for NO_3^-. (c) FEs of Cu/MnOOH (green line), pure MnOOH (orange line), and Cu/C (blue line) catalysts for NO_3^- (dot line) and NO_2^- reduction (solid line). (d) Scheme of the mechanism for eNO_3RR on the surface of Cu/MnOOH catalyst.

reach 200.27 mmol/$g_{cat.}$, which is much better than that of Cu/C (98.37 mmol/$g_{cat.}$) and pure MnOOH (80.83 mmol/$g_{cat.}$). This proves our above hypothesis that the positive shift of binding energy of Cu could enhance the adsorption of anions (NO_3^-). Moreover, in comparison with Cu/C, MnOOH, and Cu/MnOOH exhibit more positive onset potentials, thereby MnOOH can facilitate the dissociation of water and provide active hydrogen (H*) for eNO_3RR (Fig. S16 in Supporting information) [54]. Therefore, based on the above results, the present impressive activity of Cu/MnOOH is attributed to the synergistic effect between Cu NPs and MnOOH substrate, in which Cu enhances the adsorption of NO_3^- and MnOOH accelerates the hydrogenation process.

Moreover, to further explore the effect of water dissociation on eNO_3RR, H*-quenching tests are applied in the presence of *tert*-butyl alcohol (TBA) with or without NO_3^-, and the detailed experimental procedure has been provided in Supporting Information [55]. As shown in Fig. S17 (Supporting information), NH_3 yield rates decrease obviously after the addition of TBA reagent for the three catalysts, demonstrating the significant contribution of H* during eNO_3RR. Furthermore, to explore the catalytic mechanism of the catalysts, KOH (1.0 mol/L) electrolyte with NO_2^- (0.5 mol/L) is also applied to NH_3 synthesis. Fig. 4c indicates that the FEs of pure MnOOH and Cu/C catalysts increase obviously during eNO_2RR for NH_3 synthesis compared with those of eNO_3RR. This phenomenon is consistent with the previous conclusion that the reduction of adsorbed nitrate (NO_3*) to NO_2* is the main barrier for eNO_3RR [56-58]. Therefore, the synthesis of NH_3 from NO_3^- is more difficult than that from NO_2^-, which usually leads to the lower NH_3 FE for eNO_3RR than for eNO_2RR. Nevertheless, the FEs of NH_3 synthesis from eNO_3RR and eNO_2RR over Cu/MnOOH are similar, and all of them are higher than 90% in the range of −0.4 ∼ −0.8 V, suggesting that NH_3 synthesis activity of Cu/MnOOH could overcome the rate limiting step of NO_3* to NO_2* [59-61], which may also result from the enhanced adsorption ability of Cu/MnOOH to NO_3^-.

Based on the above experiments and analyses, the superior activity of Cu/MnOOH catalyst can be deduced by the following factors (Fig. 4d). Firstly, MnOOH substrate can disperse Cu NPs efficiently with ultrafine sizes, creating lots of active sites. Secondly, the electronic structure of Cu can be regulated by MnOOH substrate with a positive shift of Cu valence state, improving the adsorption ability of Cu active sites to NO_3^-. Finally, Cu/MnOOH could overcome the barrier in the step of reducing NO_3* to NO_2*. As a result, Cu/MnOOH could realize excellent eNO_3RR activity.

In summary, this work provides an efficient strategy to optimize the activity of Cu by MnOOH substrate to improve its performance of eNO_3RR. Various characterizations demonstrate the introduction of MnOOH substrate can regulate the valence states of Cu, which is positively shifted compared with the Cu/C catalyst. Adsorption experiments prove that Cu/MnOOH can enhance the adsorption capacity of NO_3^-. Additionally, electrochemical tests demonstrate that Cu/MnOOH catalyst could overcome the barrier in the step of reducing NO_3* to NO_2* efficiently. Benefiting from these factors, Cu/MnOOH achieves outstanding NH_3 synthesis performance with a superior NH_3 yield rate (55.51 mg h^{-1} cm^{-2}), high FE (96.8%), and large NH_3 partial current density (700 mA/cm^2) under ambient conditions. In addition, during long-term electrolysis, the Cu/MnOOH catalyst realizes a good stability within 20 h. The present findings highlight the potentiality of eNO_3RR as an appealing method for synthesizing NH_3 under ambient conditions, and offer a promising prospect for its application in industrial-scale production.

Declaration of competing interest

The authors declare that they have no known competing financial interests or personal relationships that could have appeared to influence the work reported in this paper.

CRediT authorship contribution statement

Hong-Rui Li: Conceptualization, Investigation, Writing – original draft. **Xia Kang:** Writing – review & editing. **Rui Gao:** Writing – review & editing. **Miao-Miao Shi:** Conceptualization, Writing – review & editing. **Bo Bi:** Writing – review & editing. **Ze-Yu Chen:** Writing – review & editing. **Jun-Min Yan:** Conceptualization, Supervision, Writing – review & editing.

Acknowledgments

This work is supported in part by National Natural Science Foundation of China (No. 51925102) and National Key R&D Program of China (No. 2022YFA1504101).

Supplementary materials

Supplementary material associated with this article can be found, in the online version, at doi:10.1016/j.cclet.2024.109958.

References

[1] S. Licht, B. Cui, B. Wang, et al., Science 345 (2014) 637–640.
[2] K.A. Brown, D.F. Harris, M.B. Wilker, et al., Science 352 (2016) 448–450.
[3] C.J. Van der Ham, M.T. Koper, D.G. Hetterscheid, Chem. Soc. Rev. 43 (2014) 5183–5191.
[4] R. Michalsky, A.M. Avram, B.A. Peterson, et al., Chem. Sci. 6 (2015) 3965–3974.
[5] D. Bao, Q. Zhang, F.L. Meng, et al., Adv. Mater. 29 (2017) 1604799.
[6] M.M. Shi, D. Bao, B.R. Wulan, et al., Adv. Mater. 29 (2017) 1606550.
[7] X. Cui, C. Tang, Q. Zhang, Adv. Energy Mater. 8 (2018) 1800369.
[8] Z. Geng, Y. Liu, X. Kong, et al., Adv. Mater. 30 (2018) 1870301.
[9] M. Wang, S. Liu, T. Qian, et al., Nat. Commun. 10 (2019) 341.
[10] Y.C. Hao, Y. Guo, L.W. Chen, et al., Nat. Catal. 2 (2019) 448–456.
[11] S. Liu, T. Qian, M. Wang, et al., Nat. Catal. 4 (2021) 322–331.
[12] M. Wang, S. Liu, H. Ji, et al., Nat. Commun. 12 (2021) 3198.
[13] M. Ghazouani, H. Akrout, L. Bousselmi, Environ. Sci. Pollut. Res. 24 (2017) 9895–9906.
[14] L. Su, K. Li, H. Zhang, et al., Water Res. 120 (2017) 1–11.
[15] P. Gayen, J. Spataro, S. Avasarala, et al., Environ. Sci. Technol. 52 (2018) 9370–9379.
[16] J.M. McEnaney, S.J. Blair, A.C. Nielander, et al., ACS Sustain. Chem. Eng. 8 (2020) 2672–2681.
[17] I. Katsounaros, M. Dortsiou, G. Kyriacou, J. Hazard Mater. 171 (2009) 323–327.
[18] M. Blarasin, A. Cabrera, I. Matiatos, et al., Sci. Total Environ. 741 (2020) 140374.
[19] G.F. Chen, Y. Yuan, H. Jiang, et al., Nat. Energy 5 (2020) 605–613.

[20] J. Li, G. Zhan, J. Yang, et al., J. Am. Chem. Soc. 142 (2020) 7036–7046.
[21] L. Mattarozzi, S. Cattarin, N. Comisso, et al., Electrochim. Acta 89 (2013) 488–496.
[22] Y. Wang, A. Xu, Z. Wang, et al., J. Am. Chem. Soc. 142 (2020) 5702–5708.
[23] Z.Y. Wu, M. Karamad, X. Yong, et al., Nat. Commun. 12 (2021) 2870.
[24] R. Jia, Y. Wang, C. Wang, et al., ACS Catal. 10 (2020) 3533–3540.
[25] X. Fu, X. Zhao, X. Hu, et al., Appl. Mater. Today 19 (2020) 100620.
[26] M. Dortsiou, G. Kyriacou, J. Electroanal. Chem. 630 (2009) 69–74.
[27] K. Chen, Z.Y. Ma, X.C. Li, et al., Adv. Funct. Mater. 33 (2023) 2209890.
[28] G. Zhang, X. Li, K. Chen, et al., Angew. Chem. Int. Ed. 62 (2023) e202300054.
[29] X. Huang, L. Huang, S.R. Babu Arulmani, et al., Environ. Res. 204 (2022) 112381.
[30] A. Kheradmand, M. Negarestani, S. Kazemi, et al., Sci. Rep. 12 (2022) 14623.
[31] Y. Xu, Y. Wen, T. Ren, et al., Appl. Catal. B 320 (2023) 121981.
[32] J. Zhao, X. Ren, X. Liu, et al., Chem. Eng. J. 452 (2023) 139533.
[33] J.X. Yao, Y.T. Zhou, J.M. Yan, et al., Adv. Energy Mater. 11 (2021) 2003701.
[34] X. Zheng, Y. Yan, X. Li, et al., J. Hazard. Mater. 446 (2023) 130679.
[35] Z. Lyu, S. Zhu, M. Xie, et al., Angew. Chem. Int. Ed. 60 (2021) 1909–1915.
[36] L. Lan, Q. Li, G. Gu, et al., J. Alloys Compd. 644 (2015) 430–437.
[37] C. Revathi, R.T.R. Kumar, Electroanalysis 29 (2017) 1481–1489.
[38] T. Gao, F. Krumeich, R. Nesper, et al., Inorg. Chem. 48 (2009) 6242–6250.
[39] Y. Li, Y. Zhang, K. Qian, et al., ACS Catal. 12 (2022) 1268–1287.
[40] T.W. van Deelen, C. Hernández Mejía, K.P. de Jong, Nat. Catal. 2 (2019) 955–970.
[41] Z. Liu, F. Shen, L. Shi, et al., Environ. Sci. Technol. 57 (2023) 10117–10126.
[42] S.B. Wang, Y.S. Xia, Z.F. Xin, et al., Catal. Commun. 173 (2023) 106564.
[43] M. Cui, H. Zhao, X. Dai, et al., ACS Sustain. Chem. Eng. 7 (2019) 13015–13022.
[44] G.P. Kim, D. Lim, I. Park, et al., J. Power Sources 324 (2016) 687–693.
[45] S. Yang, X. Song, P. Zhang, et al., J. Mater. Chem. A 3 (2015) 6136–6145.
[46] W. Sun, A. Hsu, R. Chen, J. Power Sources 196 (2011) 627–635.
[47] S. Sun, S. Wang, T. Xia, et al., J. Mater. Chem. A 3 (2015) 20944–20951.
[48] Y. Zhang, X. Dong, H. Li, et al., CrystEngComm 23 (2021) 2376–2383.
[49] H. Mizoguchi, A.W. Sleight, M.A. Subramanian, Inorg. Chem. 50 (2010) 10–12.
[50] Y. Wang, M.M. Shi, D. Bao, et al., Angew. Chem. Int. Ed. 58 (2019) 9464–9469.
[51] A.C. Nielander, J.M. McEnaney, J.A. Schwalbe, et al., ACS Catal. 9 (2019) 5797–5802.
[52] G. Jiang, M. Peng, L. Hu, et al., Chem. Eng. J. 435 (2022) 134853.
[53] Z. Song, Y. Liu, Y. Zhong, et al., Adv. Mater. 34 (2022) e2204306.
[54] Z. Lou, Y. Li, J. Zhou, et al., J. Hazard. Mater. 362 (2019) 148–159.
[55] J. Ding, W. Li, Q. Chen, et al., Inorg. Chem. Front. 10 (2023) 5762–5771.
[56] G.E. Dima, A.C.A. de Vooys, M.T.M. Koper, J. Electroanal. Chem. 554–555 (2003) 15–23.
[57] Y. Arikawa, Y. Otsubo, H. Fujino, et al., J. Am. Chem. Soc. 140 (2018) 842–847.
[58] S. Garcia-Segura, M. Lanzarini-Lopes, K. Hristovski, et al., Appl. Catal. B 236 (2018) 546–568.
[59] D. He, Y. Li, H. Ooka, et al., J. Am. Chem. Soc. 140 (2018) 2012–2015.
[60] Z. Niu, S. Fan, X. Li, et al., Appl. Catal. B 322 (2023) 122090.
[61] X. Zhang, Y. Wang, C. Liu, et al., Chem. Eng. J. 403 (2021) 126269.